View metadata, citation and similar papers at core.ac.uk

brought to you by CORE

provided by Harvard University - DASH

A Basin Redox Transect at the Dawn of Animal Life

The Harvard community has made this article openly available. Please share how this access benefits you. Your story matters.

Citation	Sperling, Erik A., Galen P. Halverson, Andrew H. Knoll, Francis A. Macdonald, and David T. Johnston. 2013. A Basin Redox Transect at the Dawn of Animal Life. Earth and Planetary Science Letters 371-372: 143–155.
Published Version	doi:10.1016/j.epsl.2013.04.003
Accessed	February 19, 2015 5:13:54 PM EST
Citable Link	http://nrs.harvard.edu/urn-3:HUL.InstRepos:12334297
Terms of Use	This article was downloaded from Harvard University's DASH repository, and is made available under the terms and conditions applicable to Open Access Policy Articles, as set forth at http://nrs.harvard.edu/urn-3:HUL.InstRepos:dash.current.terms-of-use#OAP

(Article begins on next page)

*Manuscript
Click here to view linked References

A basin redox transect at the dawn of animal life

Erik A. Sperling[1], Galen P. Halverson[2], Andrew H. Knoll[1], Francis A. Macdonald[1*], and David T. Johnston[1*]

[1]Department of Earth and Planetary Sciences, Harvard University, Cambridge, MA, USA 02138

[2]Department of Earth and Planetary Sciences/GEOTOP, McGill University, Montreal, Quebec, Canada, H3A 2A7

* Corresponding author:

Dr. David T. Johnston
Department of Earth and Planetary Sciences
Harvard University
Cambridge, MA 02138 USA
617-496-5024 (v)
617-384-7396 (f)
johnston@eps.harvard.edu

Dr. Francis A. Macdonald
Department of Earth and Planetary Sciences
Harvard University
Cambridge, MA 02138 USA
617-496-2236 (v)
617-384-7396 (f)
fmacdon@fas.harvard.edu

Keywords: Cryogenian; Fifteenmile Group; Canada; oxygen; animals; physiology

Number of words in text: 6496
Number of tables: 0
Number of Figures: 9
Number of Supplemental files: 3

Multiple eukaryotic clades make their first appearance in the fossil record between ~810 and 715 Ma. Molecular clock studies suggest that the origin of animal multicellularity may have been part of this broader eukaryotic radiation. Animals require oxygen to fuel their metabolism, and low oxygen levels have been hypothesized to account for the temporal lag between metazoan origins and the Cambrian radiation of large, ecologically diverse animals. Here, paleoredox conditions were investigated in the Fifteenmile Group, Ogilvie Mountains, Yukon, Canada, which hosts an 811 Ma ash horizon and spans the temporal window that captures the inferred origin and early evolution of animals. Iron-based redox proxies, redox-sensitive trace elements, organic carbon percentages and pyrite sulfur isotopes were analyzed in seven stratigraphic sections along two parallel basin transects. These data suggest that for this basin, oxygenated shelf waters overlay generally anoxic deeper waters. The anoxic water column was dominantly ferruginous, but brief periods of euxinia likely occurred. These oscillations coincide with changes in total organic carbon, suggesting euxinia was primarily driven by increased organic carbon loading. Overall, these data are consistent with proposed quantitative constraints on Proterozoic atmospheric oxygen being greater than 1% of modern levels, but less than present levels. Comparing these oxygen levels against the likely oxygen requirements of the earliest animals, both theoretical considerations and the ecology of modern oxygen-deficient settings suggest that the inferred oxygen levels in the mixed layer would not have been prohibitive to the presence of sponges, eumetazoans or bilaterians. Thus the evolution of the earliest animals was probably not limited by the low absolute oxygen levels that may have

characterized Neoproterozoic oceans, although these inferred levels would constrain animals to very small sizes and low metabolic rates.

1. Introduction

A number of eukaryotic groups first appear in the fossil record between the Bitter Springs isotope excursion at ~810 Ma and the Sturtian glaciation at ~715 Ma (Macdonald et al., 2010). This apparent radiation includes the first unequivocal appearances of groups such as the vase-shaped microfossils, interpreted to be related to lobose, and perhaps filose, testate amoebae (Porter and Knoll, 2000; Porter et al., 2003), scale microfossils of uncertain phylogenetic affinity (Cohen et al., 2011; Cohen and Knoll, 2012), and simple multicellular and coenocytic green algae (Butterfield et al., 1994). Interestingly, molecular clock studies suggest that the origin of animal multicellularity may have been part of this broader radiation. Studies utilizing different taxa, genes, calibration points and clock models have converged on an estimated divergence of ~800 Ma for the last common ancestor of animals (Berney and Pawlowski, 2006; Lartillot et al., 2009; Sperling et al., 2010; Erwin et al., 2011; Parfrey et al., 2011). Similar results in these studies, despite broad methodological differences, suggest this divergence estimate is approximately correct. This age finds further support in the appearance of presumed demosponge-specific biomarkers beneath ca. 635 Ma Marinoan glacial deposits (Love et al., 2009; Kodner et al., 2008); as demosponges represent a derived lineage within animals, the origin of the animal crown group must be even deeper in time. If the molecular clock ages and biomarker data are accurate, however, the lack of metazoan body and trace fossils throughout the Cryogenian and early Ediacaran periods presents a conundrum (Erwin et al., 2011). It has been hypothesized that animal body size and diversity may have been limited by relatively low levels of oxygen in the Proterozoic atmosphere and oceans. In such oceans, it is posited that animals could have been

93 restricted to small and thin body plans that did not fossilize well, with the explosion of
94 larger and ecologically diverse organisms in the late Ediacaran and Cambrian related in
95 part to increasing O_2 levels (Cloud, 1968; Rhoads and Morse, 1971; Runnegar, 1982a;
96 Knoll and Carroll, 1999). Consistent with this hypothesis, different geochemical redox
97 proxies support a directional change towards more oxygenated conditions in the latest
98 Proterozoic (reviewed by Och and Shields-Zhou, 2012; Kah and Bartley, 2011).
99 What remains highly uncertain, however, are the atmospheric and oceanic oxygen
100 concentrations prior to and during earliest animal evolution, specifically during the
101 Cryogenian period (850-635 Ma). Oxygen levels are generally assumed to have been
102 relatively low in Cryogenian oceans (e.g. Kump, 2008), but given the lack of widespread
103 paleoenvironmental documentation, the extent to which early animals were limited by
104 low oxygen levels remains unknown. Specifically, the physiological requirements of
105 small animals with low-energy lifestyles that may have characterized the Cryogenian
106 Period were likely different from the larger, more active and muscular organisms
107 preserved in Cambrian rocks. This difference needs to be considered when comparing
108 physiological requirements against the constraints provided by geochemical proxies.
109 Here, we investigate the environmental context of early animal evolution and
110 compare inferred redox constraints with the likely physiological requirements associated
111 with different grades of organization in early animal evolution. Previous iron speciation
112 and sulfur isotope studies of the pre-Sturtian Chuar Group (Canfield et al., 2008; Nagy et
113 al., 2009; Johnston et al., 2010) provide insight into Cryogenian environments, but are
114 limited to a single section deposited between ca. 770 and 742 Ma (Karlstrom et al.,
115 2000). Here we report geochemical redox proxies through seven sections along two

parallel platform-to-basin transects in the early Cryogenian Fifteenmile Group in the Tatonduk and Coal Creek inliers, Ogilvie Mountains, Yukon, Canada (Figs. 1 and 2). The Fifteenmile Group was deposited in a basin that originated during an episode of continental extension (Macdonald et al., 2012) prior to 811.51 ± 0.25 Ma, the U-Pb zircon date on a tuff in the upper portion of the Reefal Assemblage (green line in Mt. Harper Section, Figs. 3 and 6; Macdonald et al., 2010). Thus the Fifteenmile Group spans a time period that significantly preceded the earliest macroscopic multicellular forms in the Ediacaran Period (Narbonne, 2011) but overlaps with molecular-clock estimates for the divergence of crown-group animals (Erwin et al., 2011, and references above).

The paleoredox state of shale samples collected from measured stratigraphic sections was investigated using a multi-proxy approach. Specifically, iron speciation data are integrated with major-element and redox-sensitive trace element abundances, total organic carbon (TOC) percentages, and pyrite sulfur isotope values to obtain an estimate of overall water-column redox profiles. Together, the geochemical data from these stratigraphic sections provide the first early Neoproterozoic basin redox transect and give insight into paleoenvironmental conditions in this basin at the dawn of animal life. These data can then be placed in the context of other information constraining Mesoproterozoic and early Neoproterozoic oxygen levels and compared to the likely physiological requirements of early animals.

2. Geologic Background

Neoproterozoic strata in the northern Canadian Cordillera are exposed in erosional windows (‘inliers’) separated by Phanerozoic cover (Rainbird et al., 1996;

Thorkelson et al., 2005) (Fig. 1). In the Coal Creek inlier, the focus of this study, geological mapping (Fig. 2) and stratigraphic analysis indicate that Neoproterozoic extension produced a series of NNW-side down normal faults, such that the basin, at least locally, deepened towards the northwest in present-day coordinates (Macdonald et al., 2012). The Fifteenmile Group consists of lagoonal, tidal, and supertidal carbonates of the informal Gibben formation, tidal flat and deltaic deposits of the Chandindu formation, and mixed carbonates and siliciclastics of the Reefal Assemblage, which is characterized by km-scale stromatolitic reefs that transition laterally into shale-dominated, deeper water sub-basins (Macdonald et al., 2012). Shales were sampled from two parallel transects across the basin (Fig. 2), including a shorter transect passing a short distance from a stromatolite reef complex into the shale basin (Fig. 4), and a longer transect stepping further into the basin (Fig. 3). Shales were also investigated from exposures of the Reefal Assemblage ~75 km to the northwest in the Tatonduk inlier that have yielded distinctive scale microfossils (Cohen et al., 2011; Cohen and Knoll, 2012). As Fifteenmile Group strata in the Tatonduk inlier are represented only by shale interbedded with re-deposited carbonate (and no evidence for shallow-water sedimentation), these exposures are interpreted to have formed in a deeper, more distal environment than correlative sections in the Coal Creek inlier (Macdonald et al., 2012); however, displacement along poorly exposed post-Jurassic faults between the two inliers precludes precise paleogeographic reconstruction.

3. Materials and Methods

234 shale samples from logged stratigraphic sections were crushed to flour and analyzed for major and minor-element concentrations, iron speciation systematics, percent carbonate carbon and organic carbon, and pyrite sulfur isotope composition. Iron sequential extraction followed standard protocols for iron carbonate, iron oxide and magnetite extractions (Poulton and Canfield, 2005), while pyrite iron content was quantified using the chromous chloride extraction method (Canfield et al., 1986). Pyrite sulfur isotopes were determined through combustion via a Costech Elemental Analyzer linked to a Thermo Scientific Delta V in continuous flow mode (measured as SO-SO_2) using Ag_2S from the chromous chloride extraction. Major- and minor-element abundances were determined following a standard acid digestion (hydrofluoric, perchloric, hydrochloric and nitric) and measurement with ICP-AES at SGS Laboratories, Canada. Percent carbonate carbon was quantified by percent loss on acid dissolution. Total organic carbon values were determined on acidified samples by combustion within a Carlo Erba NA 1500 Analyzer attached to a Thermo Scientific Delta V Advantage isotope ratio mass spectrometer. Complete materials and methods and precision estimates for each analysis are contained in Supplementary Information.

4. Results

All geochemical measurements are reported in Supplemental Information Tables 1 and 2. Iron speciation data are plotted against the sequence stratigraphic framework for the Coal Creek inlier (Macdonald et al., 2012) in Figs. 3 and 4. Full redox proxy data are plotted against stratigraphy for the principal investigated sections including the short transect at Reefer Camp (Fig. 5), the long transect at Mt. Harper (Fig. 6), and the deepest-

184 water section at Mt. Slipper (Fig. 7). Similar plots for sections with more limited data in
185 the Coal Creek inlier (Mine Camp, East Harper and Mt. Gibben) can be found in
186 Supplemental Figs. 1-3, respectively.
187
188 4.1 *Multi-proxy estimation of paleo-redox state*
189 An estimate of water-column redox state was determined using a multi-proxy
190 approach based on iron speciation chemistry, redox-sensitive trace elements (especially
191 Mo and V) and pyrite sulfur isotope values. In iron speciation chemistry, the highly-
192 reactive pool (FeHR) consists of iron in pyrite (FeP) plus iron that is reactive to sulfide
193 on early diagenetic timescales (iron carbonates such as siderite and ankerite, and iron
194 oxides, including magnetite). The remaining unreactive pool (FeU) consists mainly of
195 iron in sheet silicates; the sum of the two pools is total iron (FeT). Key to the geological
196 application of this proxy is the observation that modern sediments deposited under oxic
197 water columns have a FeHR/FeT < 0.38, while those deposited beneath anoxic water
198 masses generally have FeHR/FeT > 0.38 [Raiswell and Canfield (1998); see also Farrell,
199 (2011), and Supplementary Information for further discussion]. The proxy can also
200 distinguish the nature of an anoxic water column based on the proportion of highly
201 reactive iron that has been sulfidized, with FeP/FeHR ratios >0.80 indicating an euxinic
202 water column, and lower ratios pointing towards ferruginous conditions (Anderson and
203 Raiswell, 2004; Poulton and Canfield, 2011).
204 Like all proxies, iron speciation has acknowledged caveats. For instance, dilution
205 by turbidites or rapid sedimentation can result in low FeHR/FeT ratios, imparting a false
206 oxic ‘signature’ to sediments deposited under an anoxic water column (Raiswell and

207 Canfield, 1998; Lyons and Severmann, 2006). Near-shore or estuarine sediments can trap
208 large amounts of iron oxides, leading to an anoxic FeHR/FeT signature for sediments
209 deposited under oxic conditions (Poulton and Raiswell, 2002). Weathering can oxidize
210 Fe^{2+} phases to Fe^{3+} phases, potentially skewing the interpretation of euxinic versus
211 ferruginous conditions (see below), although the FeHR term should remain constant
212 (Canfield et al., 2008). Consistency between independent proxies is the best test of an
213 inference, and consequently we integrated the iron speciation chemistry with other redox
214 proxies and sedimentological constraints. Redox-sensitive trace elements such as
215 vanadium and molybdenum are soluble under oxic conditions but are less soluble under
216 reducing conditions, and are scavenged by organic and inorganic particles or complex
217 with sulfide, leading to enrichments compared to average shale values (Tribovillard et al.,
218 2006). Pyrite sulfur isotope values can further inform paleoenvironmental reconstruction,
219 because sulfate reduction within a water-column where sulfate is not limiting allows
220 expression of the biological preference for lighter ^{32}S, and consequently depleted isotopic
221 compositions in the resulting pyrite with respect to seawater sulfate. Sulfate reduction
222 within sediments, on the other hand, where sulfate availability is often diffusion limited,
223 results in Rayleigh distillation, leading to pyrite values that approach seawater sulfate
224 (Johnston and Fischer, 2012).

225 In our multi-proxy framework, samples were considered likely to have been
226 deposited under an oxic water column when they showed FeHR/FeT < 0.38 (Raiswell
227 and Canfield, 1998), no enrichment in Mo and V with respect to average shales (Gromet
228 et al., 1984), and relatively enriched $\delta^{34}S$ pyrite sulfur isotope values (or not enough
229 sulfide present in the rock for measurement). Samples were considered to have been

deposited under an anoxic, ferruginous water column when they showed FeHR/FeT > 0.38, little to no Mo enrichment but often with V enrichment, and relatively enriched $\delta^{34}S$ pyrite sulfur isotope values. Finally, samples were considered to have been likely deposited under an anoxic, euxinic water column when they showed FeHR/FeT > 0.38, relatively high FeP/FeHR ratios, Mo and V enrichments, and depleted $\delta^{34}S$ pyrite sulfur isotope values.

Euxinic water columns are usually distinguished by FeP/FeHR > 0.80 or 0.70 (Poulton and Canfield, 2011), a ratio which few of these samples surpasses. Samples interpreted here as euxinic, though, clearly have much higher FeP/FeHR ratios than samples interpreted as ferruginous (see Figs. 6 and 7), and essentially no iron carbonate or magnetite. Further, these shales have very depleted $\delta^{34}S$ pyrite sulfur isotopes (to -34 ‰) and high molybdenum abundances relative to other Neoproterozoic samples (Scott et al., 2008). Two likely possibilities exist to explain these patterns: 1) these shales were deposited beneath an euxinic water column, with subsequent oxidation of pyrite to iron oxides, or (2) the shales were deposited beneath a ferruginous water column, with the zone of free sulfide accumulation essentially at the sediment-water interface. Petrographic examination of selected shales did not show widespread evidence for oxidation of pyrite, although because the samples are from outcrop and surely have suffered some alteration, it is possible that micron-scale pyrite grains beneath the limits of routine petrographic detection have been wholly or partially oxidized. In the second possibility, full access to seawater sulfate and molybdenum pools could explain the isotopic and abundance patterns for these two elements, while the shorter time interval exposed to high sulfide levels compared to a fully euxinic water column would result in

253 less sulfidization of highly-reactive iron phases. Recognizing that the development of
254 truly euxinic conditions is ambiguous and these data may represent sulfide production at
255 the sediment-water interface, inferences of euxinia in Figs. 5-7 should be treated with
256 caution.
257
258 4.2 *Sedimentary Geochemistry of the Fifteenmile Group*
259 4.2.1 *Reefer Camp transect, Coal Creek inlier*
260 Near Reefer Camp, samples from the shallow-water Chandindu formation show
261 the hallmarks of deposition under an oxic water column (Fig. 5A). Within the
262 stromatolite reef core of the Reefal Assemblage, thin black shales show high FeHR/FeT,
263 but because they show no redox-sensitive trace element enrichment, and the FeHR signal
264 is entirely dominated by iron oxides, this may represent nearshore trapping of oxides, as
265 occurs in modern settings (Poulton and Raiswell, 2002) rather than a true ocean redox
266 signal. Samples above the flooding surface atop the stromatolite reef tract have iron
267 speciation values persistently above 0.38, moderate amounts of iron carbonate, no Mo
268 enrichment and enriched pyrite sulfur isotope values, pointing to deposition under
269 ferruginous conditions. Samples from the upper part of the Reefal Assemblage signal an
270 apparent return to oxic deposition. In Fig. 5B (See Fig. 4 for the stratigraphic relationship
271 of these sections), the Chandindu formation samples again show evidence for oxic
272 deposition. Continuing upsection into shale of the Reefal Assemblage, all available
273 evidence points to deposition under a generally oxic water column.
274
275 4.2.2 *Mt. Harper, Coal Creek inlier*

Near Mt. Harper, shallow-water sediments of the Chandindu formation also show evidence for oxic deposition (Fig. 6). The Mt. Harper transect steps much farther westward into the Reefal Assemblage shale basin than the short transect at Reefer Camp, and records a thick package of black shale and foreslope carbonate that fill accommodation space associated with tectonic extension (Macdonald et al., 2012). In section GO134, the stratigraphically lowest exposed shales of the Reefal Assemblage, there is evidence for euxinic deposition. Many of these samples do not show FeHR/FeT > 0.38, but as this succession contains many siltstone turbidites and redeposited carbonates and was likely deposited rapidly during active extension (Macdonald et al., 2012), it is possible that the highly-reactive iron was diluted by high sedimentation rates. Thus a threshold for anoxia of 0.22 may be more appropriate (Raiswell and Canfield, 1998; see also discussion in Supplementary Information). These samples show relatively high FeP/FeHR, high Mo (~10-32 ppm; high for Neoproterozoic shales—Scott et al., 2008), and depleted pyrite sulfur isotope values, indicating sulfide production very near to the sediment-water interface, if not in the water column (see above). The upper half of section GO134 shows lower Mo and less depleted pyrite sulfur isotope values, potentially suggesting ferruginous or even oxic conditions. Samples at the base of section S1103 have FeHR/FeT < 0.38, no redox-sensitive trace element enrichments, and no pyrite, possibly recording deposition under oxic conditions. This is followed by a second pulse of euxinic deposition, showing similar characteristics to the samples in GO134, with elevated FeP/FeHR, high Mo abundances, and depleted pyrite sulfur isotope values. There is little evidence for euxinia above this level, with ferruginous conditions dominant in the upper Reefal Assemblage. In contrast to samples from the lower Reefal

Assemblage at Mt. Harper, where the FeHR pool is almost entirely in pyrite and iron oxides, samples from the upper Reefal Assemblage contain moderate quantities of iron carbonate. In combination with low Mo, and enriched and variable pyrite sulfur isotope values, this suggests that the upper half of the Reefal Assemblage accumulated under an anoxic, ferruginous water column. Brief and fluctuating water column oxygenation may have occurred, as evidenced by stratigraphically-variable iron speciation signatures.

4.2.3 *Mt. Slipper, Tatonduk inlier*

Iron speciation values from the Reefal Assemblage in the Tatonduk inlier (Figure 7), which represent the deepest-water setting studied (Macdonald et al., 2012), generally show FeHR/FeT > 0.38, indicating persistent deposition under an anoxic water column. Samples from the base of the section have relatively high FeP/FeHR, high Mo and depleted pyrite sulfur isotope values, pointing to euxinic deposition (or at least fluctuating euxinia). At ~90m, these proxy values decrease, indicating a transition to ferruginous conditions. A possible return to euxinia is seen at the top of the section, from strata that have yielded scale microfossils (Cohen et al., 2011).

4.2.4 *Sediment total iron contents*

The total iron to aluminum ratio is another informative redox proxy, because sedimentary iron is authigenically enriched under anoxic water columns (Lyons and Severmann, 2006). An interesting feature of shale samples from the Fifteenmile Group is that even samples considered to have been deposited under anoxic conditions have Fe/Al ratios lower than average shale (Gromet et al., 1984). Given the general concordance in

these samples of FeHR/FeT, redox-sensitive trace element abundances and pyrite sulfur isotope data, the inconsistency with Fe/Al likely indicates an intrinsic bias to either total iron or total aluminum in the Reefal Assemblage, rather than this representing oxic deposition. Total Al abundances in all shales investigated (average = 7.03 wt %) are slightly depressed relative to the North American Shale Composite (NASC; Gromet et al., 1984; 8.94 wt %). In contrast, total Fe (average = 2.43 wt %) is significantly reduced relative to NASC (4.43 wt %), especially considering that basinal samples interpreted as anoxic should be enriched in iron. Some Reefal Assemblage shales are exceptionally low in total iron (<1 weight percent), and have very high FeHR/FeT ratios indicating a near-absence of detrital iron-silicates. Dilution by carbonate may explain some of the low iron contents, as some samples are slightly calcareous (to ~30-40%, average 9.45% ± 9.50), Supplementary Table 1) but low iron contents persist in shale samples that have essentially no carbonate (e.g. GO134 and S1103 sections). Open-system diagenesis could have potentially affected these rocks, although even the marls would have had very low permeability. Further, the main effect of diagenesis in carbonates is to add iron (Brand and Veizer, 1980), which is unlikely given the low overall amounts of acetate-extractable iron (average 0.13 weight percent) and the lack of a relationship between percent carbonate and acetate-extractable iron ($R^2 = 0.062$). Another possibility is that the provenance was extremely weathered, iron-free material. However, Chemical Index of Alteration (CIA; Nesbitt and Young, 1982) values average ~70 throughout the dataset, indicating a fairly unweathered provenance. A few values in the 75-85 range suggest a weathered source for those samples, but overall there is no obvious correlation between CIA and total iron. Thus, while several factors may explain some low iron values, none

345 can explain all low values. We note that some other Neoproterozoic sections show
346 anomalously low FeT/Al (e.g. Sahoo et al., 2012); further study is needed to determine if
347 these are local, basin-level effects or an as-yet-unexplained aspect of the Neoproterozoic
348 iron cycle.
349
350 4.2.5 *Redox proxy data and sediment organic carbon contents*
351 Sediment TOC results vary consistently compared to multi-proxy inferences of
352 redox state (Fig. 8). Sediments likely deposited under an oxic water column have low
353 organic carbon abundances (average = 0.31% ± 0.49 weight percent; median = 0.19%),
354 whereas those inferred to have been deposited beneath a ferruginous water column have
355 higher sediment TOC values (average = 0.66% ± 1.37; median = 0.28%). And sediments
356 likely deposited beneath euxinic conditions show much greater TOC (average = 2.87% ±
357 1.49; median = 2.63. Thus, these data are consistent with the hypothesis that the
358 development of euxinic conditions in Neoproterozoic basins is primarily driven by the
359 degree of organic carbon loading and the exhaustion of more energetically-favorable
360 electron acceptors than sulfate (e.g. Fe^{3+}) (Johnston et al., 2010).
361
362 4.2.6 *Redox proxy data and water depth*
363 Redox proxy data show a consistent pattern with respect to sedimentological
364 structures that indicate relative water depth. In particular, all occurrences of hummocky
365 cross-stratified sandstones encased within shale, which indicate deposition above storm
366 wave base, show evidence for oxic deposition (Fig. 3-7). In other words, the surface
367 mixed layer in the basin appears to be oxygenated, at least during storms. While the depth

of storm wave base varies among basins (Peters and Loss, 2012), these data indicate that in this basin, the water column in direct contact with the atmosphere remained oxic. Oxygenated conditions may extend slightly deeper, as some sediments likely deposited below storm wave base (such as shales basinward of the stromatolite reef at Reefer Camp, Fig. 5B) still indicate oxic conditions. A few brief intervals of oxygenated conditions, or fluctuating anoxia, persist deeper into the Coal Creek inlier shale basin as recorded in the Mt. Harper (Fig. 6) and Mine Camp (Supplementary Fig. 1) sections, but the majority of these deeper-water sediments record anoxic conditions. The deepest-water section at Mt. Slipper in the Tatonduk inlier (Fig. 7), which shows no evidence for wave activity, is persistently anoxic. Thus, there is a clear redox structure to the basin, with an oxygenated surface layer where the sediments are in contact with the atmosphere (storm wave base), and anoxic conditions below this depth.

5. Discussion

5.1 *Fifteenmile Group redox structure in a global context*

Quantitative constraints on Proterozoic oxygen levels are notoriously difficult to obtain (Kump, 2008). O_2 levels must have been above 0.001% present atmospheric levels (PAL), the limit imposed by the disappearance of mass-independent fractionation of sulfur isotopes at ~2.45 Ga (Farquhar et al., 2000; Pavlov and Kasting, 2002). Two other constraints have been proposed for mid-Proterozoic O_2 (Kump, 2008). First, anoxic deep oceans likely require atmospheric O_2 to be less than 40% PAL (Canfield, 2005). Second, it has been proposed that iron is only retained in lithified soil horizons, and it has been since the Paleoproterozoic, when O_2 is greater than 1% PAL (Holland and Beukes, 1990).

These limits on Proterozoic O_2 have caveats, and it has even been hypothesized that levels may not have been dramatically different from the Phanerozoic (Butterfield, 2009). Nonetheless, it is notable that the basin redox transect of the Fifteenmile Group is consistent with proposed quantitative limits (Kump, 2008). Indeed, the basin redox structure of the Fifteenmile Group is similar in many ways to that of the Mesoproterozoic Roper Group in Australia (Shen et al., 2003), with an oxygenated shelf overlying anoxic basinal waters. Although there are local drivers for anoxia (Tyson and Pearson, 1991), the available basin redox transects point to extensive subsurface anoxia in the Proterozoic oceans, sustained over hundreds of meters of stratigraphic section. This clearly differs from Phanerozoic ocean anoxic events (Campbell and Squire, 2010), indicating a different driver and implying lower atmospheric O_2 than the modern. Placing minimum constraints on global atmospheric pO_2 levels from local iron speciation data is difficult, but shallow-water facies in the Fifteenmile Group record oxic deposition, as do samples from the shale basin just off the reef margin at Reefer Camp (Fig. 5), and some samples from deeper in the shale basin at Mt. Harper (Fig. 6) and Mine Camp (Supplementary Fig. 1), implying enough atmospheric oxygen to counteract strong benthic reductant fluxes in a basin otherwise prone to euxinia (cf. Kump et al., 2005).

In sum, although there is clear need to study more basins, and develop new global redox proxies and models, the basin redox transect of the Fifteenmile Group is consistent with proposed constraints on Proterozoic oxygen levels as being <40% and >1% PAL (Kump, 2008). We apply these bounds for comparison with the physiological requirements of early animals.

5.2 Physiological requirements of early animals

The consistency of previously proposed constraints on atmospheric oxygen with the basin redox transect of the Fifteenmile Group prompts the question of whether such oxygen levels would have prohibited the evolution of animal, eumetazoan or bilaterian body plans. A common assumption in attempts to link late Precambrian oxygenation and biospheric evolution is that animals have high respiratory demands. While metazoans do have a clear and definite requirement for oxygen, they are not a monolithic group, and the oxygen requirements for any given organism varies widely based on size, metabolism, and the presence or absence of a circulatory system (Vaquer-Sunyer and Duarte, 2008). Hypotheses relating geochemical change to early animal evolution must therefore compare inferred changes against the explicit body plans, ecological strategies and taxonomic groups presumed to be affected. Determining the physiological requirements of ancient organisms has obvious uncertainty, but can be accomplished through analogy with living representatives (Knoll et al., 2007), and thus it is possible to make general statements about the likely oxygen requirements of Precambrian animals.

5.2.1 *Diploblastic metazoans*

Whether sponges are monophyletic (Philippe et al., 2009) or paraphyletic (Sperling et al., 2009), they are certainly the sister group or grade of all other animals (Philippe et al., 2011). Moving up the metazoan phylogenetic tree, the exact relationships of cnidarians, ctenophores and placozoans to bilaterians are unclear, but all are likely more closely related to bilaterians than they are to sponges (Philippe et al., 2011). Importantly, all these animals (diploblasts) are characterized by only two epithelial cell

437 layers, with the space between layers filled largely with metabolically-inert material (e.g.
438 mesohyl in sponges, mesoglea in cnidarians). From a respiratory point of view, then,
439 essentially every cell in a diploblastic metazoan is in direct contact with seawater
440 (Ruppert et al., 2004). Thus, the theoretical oxygen limit for diploblastic animals will not
441 differ from that of a single-celled eukaryote, barring two minor differences. First, for
442 unicellular eukaryotes, diffusion of oxygen into the cell can occur across the entirety of
443 its surface, whereas diffusion into a sheet of cells cannot occur at cell-cell contacts.
444 Second, animals have a collagenous extracellular matrix, and molecular oxygen is
445 required for the formation of hydroxyproline in collagen (Fujimoto and Tamiya, 1962;
446 Prockop et al., 1962). Using the *Km* for the proline hydroxylase system of chick embryos,
447 Towe (1970) suggested oxygen levels of ~3% PAL would be required for collagen
448 synthesis. However, Rhoads and Morse (1971) cogently noted that collagen-rich
449 invertebrates are found at oxygen levels beneath this value (see also discussion below on
450 modern oxygen minimum zones), suggesting that the oxygenase requirements of a
451 terrestrial vertebrate cannot be applied to marine invertebrates. Further, collagen is now
452 known to exist in fungi (Celerin et al., 1996; Wang and St. Leger, 2006) and
453 choanoflagellates (King et al., 2008--although the homology of both to metazoan
454 collagens remains uncertain), which suggests collagen may have been present in the last
455 common ancestor of opisthokonts. If so, any oxygen requirement for collagen synthesis
456 was met far earlier than the origin of animals.
457 In the fossil record, clear eukaryotic organisms are found at ~1800 Ma, and
458 several lineages of multicellular eukaryotes, which would also have been subject to the
459 same constraint as early animals of limited diffusion at cell-cell contacts, are found in

Mesoproterozoic rocks (Runnegar, 1991; Knoll et al., 2006). The presence of these organisms long before the Cryogenian implies that any physiological oxygen threshold for the body plans that characterized the earliest (diploblastic) period of early animal evolution must have been surpassed far prior to the origin of animals themselves.

5.2.2 *Bilaterian metazoans- theoretical lower oxygen limits*

In contrast to diploblasts, which have sheets of cells separated by inert material, bilaterian (triploblastic) organisms have metabolically-active cells in three-dimensions (Knoll, 2011). Body size (and the ability of the organism to exist at a given oxygen concentration) is consequently limited by the ability to maintain functional internal oxygen levels, either through pure diffusion or through a blood vascular system (BVS). The implications of this constraint under hypothetical Precambrian oxygen levels have been extensively discussed (e.g. Raff and Raff, 1970; Runnegar, 1982a,b; 1991; Catling et al., 2005; Payne et al., 2010). Using a theoretical framework for the diffusion of oxygen into an idealized animal (Alexander, 1971), these studies have demonstrated that low oxygen levels will restrict bilaterians to small, thin body plans. What has not been asked in these theoretical calculations is what oxygen levels will prohibit the existence of bilaterian body plans.

Superficially, this question would seem to hinge on the nature of the last common ancestor of bilaterians (consider Carroll et al., 2001, versus Erwin and Davidson, 2002), specifically whether this ancestor was a complex, coelomate organism with a heart and BVS, or a much simpler organism that transported oxygen through pure diffusion. However, as noted by Budd and Jensen (2000), due to structural size requirements,

notably the physical space required to fit a functional BVS, this transport system is not present in modern organisms less than ~3mm in size. Following the framework of Alexander (1971; see Supplementary Information for details), we estimate that the most likely minimal oxygen requirement for a 3 mm-long x 67 μm-wide worm with a circulatory system, such as an annelid, is ~0.14% PAL (Fig. 9). The most likely minimal oxygen requirements for a 600 x 25 μm diameter worm limited by pure diffusion, such as a nematode, is ~0.36% PAL (Fig. 9)—note that these values are with respect to ambient dissolved oxygen concentrations and do not consider temperature or salinity effects on the dissolution of oxygen in water. The estimated oxygen requirements for these two hypothetical ancestors differ slightly, but their broad similarity and the overlap in sensitivity analyses (Fig. 9) suggests that pure diffusion and a BVS likely represent optimal designs below and above this size threshold.

Although there are uncertainties in the optimal values for the parameters in the equations governing oxygen requirements (see Supplementary Information), three facts suggest the values described above represent conservative estimates for the minimum oxygen concentrations necessary to sustain bilaterians. First, for the bilaterian limited by pure diffusion, a sensitivity analysis (Fig. 9 and Supplementary Table 7) demonstrates that one of the most important terms at very low oxygen levels is the minimum cellular oxygen concentration. This will be a small, but non-zero, number (Raff and Raff, 1970). Raff and Raff (1970) used a value of $1/10^{th}$ the shared *Km* of yeast and mammalian cytochrome oxidase. Here, rather than adopting an arbitrary but likely more accurate fractional value, we use the shared yeast-mammal *Km* (Chance, 1957) as our ‘most likely’ value for this parameter (note that investigated invertebrate cytochrome oxidases

506 have a similar value (e.g. Gnaiger et al., 2000)). This ensures that the most important
507 parameter in the model is an over-estimate. Second, for the hypothetical ancestor with a
508 circulatory system, we assumed the organism did not have respiratory pigments.
509 Although the homology of metazoan respiratory pigments is unclear (Terwilliger, 1998),
510 their presence in this hypothetical last common bilaterian ancestor would greatly increase
511 diffusion rates. Thus, our assumption that respiratory pigments were absent again results
512 in a conservative estimate. Finally, and most importantly, these theoretical calculations
513 assume a perfectly tubular organism (Alexander, 1971). Such an organism does not exist,
514 as real animals have body wall rugosities, gills, and other structures that dramatically
515 increase diffusive surface area with respect to volume; even the gut is a gas-exchange
516 organ. Consequently, these 'most likely' values and the sensitivity analyses are not
517 intended to yield a precise number. Rather, these models provide an indication of the
518 lower bound of oxygen levels necessary to preclude the bilaterian body plan from
519 Proterozoic oceans. No matter the complexity of the last common ancestor of bilaterians,
520 theoretical modeling suggests the bilaterian body plan was unlikely to have been
521 prohibited unless O_2 levels were < 0.4% PAL.
522
523 5.2.3 *Bilaterian metazoans- empirical lower oxygen limits*
524 These theoretical calculations can be tested with empirical observations of the
525 oxygen limits of bilaterians in modern oxygen-minimum zones (OMZs). Unlike the biota
526 on shelves or in regions of anthropogenic eutrophication that show deleterious oxygen
527 responses at relatively minor oxygen depletions (Diaz and Rosenburg, 1995; Levin et al.,
528 2009), OMZs have experienced geologically long-lasting dysoxic- to anoxic conditions,

allowing the fauna to adapt to these levels and providing an excellent analogue for Precambrian oceans with persistently low oxygen levels. It should be noted that organisms in modern OMZs have likely secondarily adapted to these environments rather than originating in them. Thus, the type of adaptations allowing organisms to inhabit these environment must be considered. For example, organisms with extreme metabolic adaptations, such as amitochondriate loriciferans living in an euxinic Mediterranean basin (Danovaro et al., 2010), cannot inform us about Precambrian animal evolution, as the transformation of the mitochondria into a hydrogenosome was certainly not a primitive feature. Most of the adaptations allowing bilaterians to inhabit modern low-oxygen environments, though, appear to lie in their very small, thin body plans (with high surface-area to volume ratios for increased diffusion) and enlarged respiratory organs (Levin, 2003; Gooday et al., 2010; Jeffreys et al., 2012; Lamont and Gage, 2000; Neira et al., 2001)—that is, with morphological adaptations that would have been possible, and perhaps likely, in early bilaterians. Consequently these animals can provide a useful analogue for Precambrian animal life in low-oxygen conditions.

In using OMZs as Precambrian analogues, it has long been recognized that the faunas are characterized by such small, thin, body plans (Rhoads and Morse, 1971). What has emerged in the four decades of oceanographic research since Rhoads and Morse's seminal paper is just how little oxygen is actually required by bilaterian animals. It is now clear that non-chemosymbiotic benthic macrofaunal (retained on 0.3 mm sieves) bilaterians can and do live in Rhoads and Morse's 'azoic' zone of <0.10 mL/L oxygen[1]

[1] A difficulty in interdisciplinary research on the biological effects of differing oxygen levels is the use of different units by different research communities (Hofmann et al.,

(Levin, 2003; Gooday et al., 2010; Levin et al., 2000; Palma et al., 2005; Zettler et al., 2009; Levin et al., 1991; Levin et al., 2002; Ingole et al., 2010), often with densities of hundreds to thousands of animals per square meter. Bilaterian faunas can even be found as low as 0.02 ml/L O_2, equivalent to ~0.3% of modern surface ocean levels (assuming a normal surface ocean concentration of ~6 mL/L) in the OMZ off Chile (Palma et al., 2005), Peru (Levin et al., 2002) and the Bay of Bengal (R. Akkur, pers. comm.). The exact oxygen concentrations actually required to exclude bilaterians are likely even lower, these oxygen measurements are determined from O_2 sensors or seawater samples from CTD casts collected several meters (~5 m) above the seafloor. The oxygen levels at which bilaterians are recorded (namely 0.02 mL/L) approach the detection limit of the Winkler titration technique (Paulmier et al., 2006), and CTD cast values generally over-estimate in-situ benthic conditions (Breur et al., 2009). Thus, both theoretical calculations and empirical observations in modern OMZs suggest the presence of bilaterians would not have been limited unless atmospheric O_2 was considerably less than 1% PAL, and likely less than 0.4% PAL.

7. Conclusions

Geochemical transects of the ~800 Ma Fifteenmile Group in the Ogilvie Mountains document shallow-water facies characterized by low FeHR/FeT, a lack of enrichment in redox-sensitive trace elements, and relatively heavy and variable pyrite sulfur isotope values. Deeper-water facies (those deposited below storm wave base) are characterized by FeHR/FeT > 0.38, enrichment in redox-sensitive trace elements, and

2011). For consistency here we report oxygen levels as in the benthic ecology literature (mL/L). For reference 0.01 mL/L ≈ 0.44 *u*mol/kg ≈ 0.014 mg/L ≈ 0.4 matm.

572 more depleted pyrite sulfur isotope values. Overall, this points towards an oxygenated
573 surface layer, down to storm wave base, overlying a generally anoxic deep basin.
574 Fluctuations between euxinic and ferruginous conditions sub-storm wave base appear to
575 have been controlled by variations in organic carbon loading. As proxies like iron
576 speciation and redox-sensitive trace elements provide evidence of local environments,
577 more geochemical studies from other basins are necessary to begin building the global
578 picture of redox heterogeneity. Further, the development of quantitative global redox
579 tracers and better modeling are needed to place tighter constraints on the history of
580 oxygen on Earth. Nonetheless, the Fifteenmile Group redox structure is comparable to
581 that of a well-characterized Mesoproterozoic basin (Shen et al., 2003)—albeit with more
582 evidence for ferruginous conditions-- and both basins are consistent with broad estimates
583 for atmospheric oxygen levels between 1 and 40% PAL (Kump, 2008).
584 Comparing these likely O_2 levels with the estimated physiological requirements of
585 early animals suggests that sufficient atmospheric oxygen, even for mobile bilaterians,
586 was present well in advance of the origin of animals. Unless early Neoproterozoic oxygen
587 levels were substantially < 1% PAL, and likely < 0.4% PAL, atmospheric oxygen levels
588 would not have prohibited the sponge, eumetazoan and bilaterian body plans. This
589 conclusion does not imply that animals necessarily lived in the Fifteenmile basin, but
590 rather that global O_2 levels were likely adequate for the presence of animals. Notably, this
591 does not negate the possibility of an oxygenation event around the Sturtian glaciation
592 (Planavsky et al., 2010; Frei et al., 2009), or the use of oxygenated ‘oases’ beneath
593 photosynthetic mats by the earliest trace makers in the geological record (Gingras et al.,

2011), but it does suggest that such conditions were not necessary for the origin of either animals or bilaterians.

It is important to remember, though, that while low Precambrian oxygen levels would not have prohibited animals, including bilaterians, the environmental milieu would still have exerted a strong effect on life. Most importantly, low oxygen certainly would have constrained these organisms to very small and thin body plans with little metabolic scope (Raff and Raff, 1970; Runnegar, 1982a, b; Payne et al., 2010). Faunas in modern low-O_2 OMZ analogues have very small body sizes, reduced diversity, and simple food webs (Levin, 2003; Gooday et al., 2009; Sperling et al., in review). In other words, although all available data suggests bilaterians *can* live down to 1% PAL or less, the fauna would be limited to a select few—those organisms that were a couple millimeters in length and had low-energy lifestyles. Thus, while no oxygenation event need be invoked to explain the origin of animals or bilaterians themselves, the hypothesized end-Neoproterozoic oxygenation event (the timing and magnitude of which remains debated—Kah and Bartley, 2011; Och and Shields-Zhou, 2012) may still have played a role in the later Ediacaran diversification of macroscopic animals and the Cambrian 'Explosion' (e.g. Runnegar, 1982a; Rhoads and Morse, 1971; Knoll and Carroll, 1999). Although Cambrian diversification was certainly multifaceted (Erwin et al., 2011), a latest Proterozoic increase in oxygen levels could have allowed for an increase in both size and metabolic scope, including potentially the advent of predation, a metabolically-costly feeding strategy.

ACKNOWLEDGEMENTS

We thank J. Strauss, A. Eyster, E. Smith and S. Braun for assistance in the field, A. Masterson, E. Beirne, and B. Gill for technical assistance, G. Eischeid, G. Resendiz, D. Cole and N. Waldo for help with sample preparation and laboratory analyses, P. Cohen, P. Girguis, J. Payne, K. Peterson, J. Strauss, L. Levin and C. Frieder for helpful discussion, and D. Fike and two anonymous reviewers for insightful comments. We thank Fireweed Helicopters for safe and reliable transportation, and the Yukon Geological Survey for field support. We thank D. Schrag, Harvard University Laboratory for Chemical Oceanography, and S. Poulton, Newcastle University, for help with sample analysis in their labs. EAS is supported by an Agouron Institute post-doctoral fellowship. DTJ is supported by NSF EAR/IF, NASA Exobiology, and Harvard University. EAS, AHK, DTJ and FAM thank the NASA Astrobiology Institute for support.

FIGURE CAPTIONS

Fig. 1- Location map of the Coal Creek and Tatonduk inliers, Yukon Territory, Canada, with stars marking the location of the inliers.

Fig. 2- Geological map of the Coal Creek inlier, Ogilvie Mountains, Yukon Territory, showing sections (in red) studied in this paper. The stratigraphic framework for basin transects A – A’ and B – B’ are found in Fig. 3 and 4. The units studied as part of this paper are the informal Gibben formation, Chandindu formation and Reefal Assemblage of the Fifteenmile Group. Geological mapping by Macdonald et al. (2012).

Fig. 3- Stratigraphic framework and iron speciation chemistry for transect A – A' at Mine Camp, Mt. Harper and Mt. Gibben, Coal Creek inlier. Iron speciation chemistry (specifically the ratio of highly reactive iron (FeHR) to total iron (FeT)) from fine-grained siliciclastic rocks is plotted against the stratigraphic columns. Vertical line on iron speciation plots denotes a ratio of 0.38, with samples having higher ratios considered to have been deposited under an anoxic water column, and samples with lower ratios likely to have been deposited under an oxic water column. Complete redox proxy data for individual sections is found in Fig. 6 (Mt. Harper), Supplemental Fig. 1 (Mine Camp), Supplemental Fig. 2 (East Harper) and Supplemental Fig. 3 (Mt. Gibben). *m*- mud; *si*-silt; *ms*- medium sand; *cs*- coarse sand; *cg*- conglomerate. *Gib.* = Gibben formation.

Fig. 4- Stratigraphic framework and iron speciation chemistry for transect B – B' at Reefer Camp, Coal Creek inlier. Sections are located 5 km apart and record a transition in the Reefal Assemblage from a stromatolite reef complex into a deeper-water shale basin. Iron speciation chemistry (specifically the ratio of highly reactive iron (FeHR) to total iron (FeT)) from fine-grained siliciclastic rocks is plotted against the stratigraphic columns. Vertical line on iron speciation plots denotes a ratio of 0.38, with samples having higher ratios considered to have been deposited under an anoxic water column, and samples with lower ratios likely to have been deposited under an oxic water column. Complete redox proxy data for individual sections at Reefer Camp is found in Fig. 5. Legend for stratigraphic columns and sediment type abbreviations as in Fig. 3. Abbreviations: *W.* = Wernecke Supergroup, *Gib.* = Gibben formation, *Cha.* = Chandindu formation.

Fig. 5- Redox proxy data from sections B’ (Fig. 5A) and B (Fig. 5B) at Reefer Camp, Coal Creek inlier. From left to right, proxy data plotted and their respective relevant baseline data denoted by vertical red lines are: highly reactive to total iron (FeHR/FeT; 0.38), pyrite iron to highly reactive iron (FeP/FeHR; 0.80), total iron to total aluminum (FeT/Al; 0.50), molybdenum (2.6 ppm), vanadium (130 ppm), pyrite sulfur isotope values (0 ‰), and weight percent total organic carbon. Relative base level curve from sequence stratigraphic study of Macdonald et al. (2012). The far right column is a subjective estimate of water column redox state based on the multi-proxy data, and is meant to represent general trends rather than an estimate for every point. Euxinia(?) denotes uncertainty regarding whether these samples represent deposition under a truly euxinic water column or a ferruginous water column with sulfide production at or near the sediment-water interface (see text). Legend for stratigraphic column and formation name abbreviations as in Fig. 3 and 4.

Fig. 6- Redox proxy data from the Mt. Harper section, Coal Creek inlier. This figure is a composite section from the Mt. Harper area (Fig. 2). Redox proxy data and their relevant baseline values (marked by vertical red lines) as in Figure 5. Relative base level curve from sequence stratigraphic study of Macdonald et al. (2012). The far right column is a subjective estimate of water column redox state based on the multi-proxy data, and is meant to represent general trends rather than an estimate for every point. Euxinia(?) denotes uncertainty regarding whether these samples represent deposition under a truly euxinic water column or a ferruginous water column with sulfide production at or near

685 the sediment-water interface (see text). Legend for stratigraphic column and formation
686 name abbreviations as in Fig. 3 and 4.
687
688 **Fig. 7-** Redox proxy data from the Mt. Slipper section, Tatonduk inlier. Redox proxy data
689 and their relevant baseline values (marked by vertical red lines) as in Figure 5. Relative
690 base level curve from sequence stratigraphic study of Macdonald et al. (2012). The far
691 right column is a subjective estimate of water column redox state based on the multi-
692 proxy data, and is meant to represent general trends rather than an estimate for every
693 point. Euxinia(?) denotes uncertainty regarding whether these samples represent
694 deposition under a truly euxinic water column or a ferruginous water column with sulfide
695 production at or near the sediment-water interface (see text). Legend for stratigraphic
696 column and formation name abbreviations as in Fig. 3 and 4. Scale microfossils described
697 by Cohen et al. (2011) are found at the top of the Reefal Assemblage at this locality.
698
699 **Fig. 8-** Boxplot analysis of total organic carbon weight percentages for samples
700 determined likely to have been deposited under a ferruginous and euxinic water column.
701 Bottom-water redox state for each sample was estimated using a multi-proxy framework
702 including iron speciation data, redox-sensitive trace elements and pyrite sulfur isotope
703 values (see text for details). Samples designated as euxinic may represent sulfide
704 accumulation at the sediment-water interface rather than true water-column euxinia (see
705 text). The box represents the 25^{th} and 75^{th} percentiles, the thick horizontal line represents
706 the median, and the whiskers represent minimum and maximum values. An extreme

707 outlier in the ferruginous set (E1002- 470.4; 9.87 wt %) was included in the boxplot
708 calculations but not graphed.
709
710 **Fig. 9-** Theoretical minimum oxygen requirements for the last common ancestor (LCA)
711 of bilaterians, following the equations governing the diffusion of oxygen into an
712 organism from Alexander (1971) and modified by Payne et al. (2010). Estimates were
713 made for two potential body plans characterizing the bilaterian LCA, a 600 *u*m long
714 worm limited by pure diffusion, and a 3-mm long worm with a circulatory system. 'Most
715 likely' values represent values estimated from optimal values for all parameters (see
716 Supplemental Information). Minimum and maximum values were derived from the
717 literature for each parameter and global minimum and maximum values were estimated.
718 A sensitivity analysis was then conducted for each parameter by varying that parameter
719 between minimum and maximum values while keeping all other parameters at their 'most
720 likely' values. All estimates for oxygen requirements are far less than the 1% of Present
721 Atmospheric Levels indicated by canonical views of atmospheric oxygen levels in the
722 Proterozoic (Kump, 2008). Lowest row for extant mobile bilaterians shows the current
723 lower oxygen limit at which bilaterians are found in the modern ocean (0.02 mL/L $O_2 \approx$
724 0.33% of modern surface ocean levels assuming a normal surface ocean level of 6 mL/L).
725 Bilaterians are found at these levels off the coasts of Peru, Chile, and in the Bay of
726 Bengal. This oxygen level may represent an overestimate due to the methodology used to
727 measure oxygen in most benthic ecology studies (Breur et al., 2009 and see text).
728
729 **References**
730

731 Alexander, R.M.N., 1971. Size and shape. Edward Arnold, London. p. 1-59.
732 Anderson, T.F., Raiswell, R., 2004. Sources and mechanisms for the enrichment of
733 highly reactive iron in euxinic Black Sea sediments. American Journal of Science
734 304, 203-233.
735 Berney, C., Pawlowski, J., 2006. A molecular time-scale for eukaryote evolution
736 recalibrated with the continuous microfossil record. Proceedings of the Royal
737 Society London B 273, 1867-1872.
738 Brand, U., Veizer, J., 1980. Chemical diagenesis of a multicomponent carbonate
739 system—1: trace elemens. Journal of Sedimentary Petrography 50, 1219-1236.
740 Breur, E.R., Law, G.T.W., Woulds, C., Cowie, G.L., Shimmield, G.B., Peppe, O.,
741 Schwartz, M., McKinlay, S., 2009. Sedimentary oxygen consumption and
742 microdistribution at sites across the Arabian Sea oxygen minimum zone (Pakistan
743 margin). Deep-Sea Research II 56, 296-304.
744 Budd, G.E., Jensen, S., 2000. A critical reappraisal of the fossil record of the bilaterian
745 phyla. Biological Reviews 75, 253-295.
746 Butterfield, N.J., 2009. Oxygen, animals and oceanic ventilation: an alternative view.
747 Geobiology 7, 1-7.
748 Butterfield, N.J., Knoll, A.H., Swett, K., 1994. Paleobiology of the Neoproterozoic
749 Svanbergfjellet Formation, Spitsbergen. Lethaia 27, 76-76.
750 Campbell, I.H., Squire, R.J., 2010. The mountains the triggered the Late Neoproterozoic
751 increase in oxygen: The second Great Oxidation Event. Geochimica et
752 Cosmochimica Acta 74, 4187-3206.
753 Canfield, D.E., 2005. The early history of atmospheric oxygen: homage to Robert M.
754 Garrels. Annu. Rev. Earth Planet. Sci. 33, 1-36.
755 Canfield, D.E., Poulton, S.W., Knoll, A.H., Narbonne, G.M., Ross, G., Goldberg, T.,
756 Strauss, H., 2008. Ferruginous conditions dominated later Neoproterozoic deep-
757 water chemistry. Science 321, 949- 952.
758 Canfield, D.E., Raiswell, R., Westrich, J.T., Reaves, C.M., Berner, R.A., 1986. The use
759 of chromium reduction in the analysis of reduced inorganic sulfur in sediments
760 and shale. Chemical Geology 54, 149-155.
761 Carroll, S., Grenier, J., Weatherbee, S., 2001. From DNA to Diversity: Molecular
762 Genetics and the Evolution of Animal Design (Malden, MA: Blackwell Science).
763 Inc.
764 Catling, D.C., Glein, C.R., Zahnle, K.J., McKay, C.P., 2005. Why O_2 Is Required by
765 Complex Life on Habitable Planets and the Concept of Planetary "Oxygenation
766 Time". Astrobiology 5, 415-438.
767 Celerin, M., Ray, J., Schisler, N., Day, A., Stetler-Stevenson, W., Laudenbach, D., 1996.
768 Fungal fimbriae are composed of collagen. The EMBO journal 15, 4445-4453.
769 Chance, B., 1957. Cellular oxygen requirements. Federation Proceedings 16, 671-680.
770 Cloud Jr, P.E., 1968. Atmospheric and hydrospheric evolution on the primitive Earth.
771 Science 160, 729-736.
772 Cohen, P.A., Schopf, J.W., Butterfield, N.J., Kudryavtsev, A.B., Macdonald, F.A., 2011.
773 Phosphate biomineralization in mid-Neoproterozoic protists. Geology 39, 539-
774 542.
775 Cohen, P.A., Knoll, A.H., 2012. Neoproterozoic scale microfossils from the Fifteenmile
776 Group, Yukon Territory. Journal of Paleontology 86, 775-800.

777 Danovaro, R., Dell'Anno, A., Pusceddu, A., Gambi, C., Heiner, I., Kristensen, R.M.,
778 2010. The first metazoa living in permanently anoxic conditions. BMC Biology 8,
779 30.
780 Diaz, R.J., Rosenberg, R., 1995. Marine benthic hypoxia: a review of its ecological
781 effects and the behavioural responses of benthic macrofauna. Oceanography and
782 Marine Biology Annual Review 33, 245-303.
783 Erwin, D.H., Davidson, E.H., 2002. The last common bilaterian ancestor. Development
784 129, 3021-3032.
785 Erwin, D.H., Laflamme, M., Tweedt, S.M., Sperling, E.A., Pisani, D., Peterson, K.J.,
786 2011. The Cambrian conundrum: Early divergence and later ecological success in
787 the early history of animals. Science 334, 1091-1097.
788 Farquhar, J., Bao, H., Thiemens, M., 2000. Atmospheric influence of earth's earliest
789 sulfur cycle. Science 289, 756-758.
790 Farrell, U.C., 2011. Taphonomy and Paleoecology of Pyritized Trilobite Faunas from
791 Upstate New York. Yale University, New Haven, CT, p. 1-430.
792 Frei, R., Gaucher, C., Poulton, S.W., Canfield, D.E., 2009. Fluctuations in Precambrian
793 atmospheric oxygenation recorded by chomium isotopes. Nature 461, 250-253.
794 Fujimoto, D., Tamiya, N., 1962. Incorporation of ^{18}O from air into hydroxyproline by
795 chick embryo. Biochemical Journal 84, 333-335.
796 Gingras, M., Hagadorn, J.W., Seilacher, A., Lalonde, S.V., Pecoits, E., Petrash, D.,
797 Konhauser, K.O., 2011. Possible evolution of mobile animals in association with
798 microbial mats. Nature Geoscience 4, 372-375.
799 Gnaiger, E., Mendez, G., Hand, S.C., 2000. High phosphorylation efficiency and
800 depression of uncoupled respiration in mitochondria under hypoxia. Proceedings
801 of the National Academy of Sciences 97, 11080-11085.
802 Gooday, A.J., Bett, B.J., Escobar, E., Ingole, B., Levin, L.A., Neira, C., Raman, A.V.,
803 Sellanes, J., 2010. Habitat heterogeneity and its influence on benthic biodiversity
804 in oxygen minimum zones. Marine Ecology 31, 125-147.
805 Gooday, A.J., Levin, L.A. da Silva, A.A., Bett, B.J., Cowie, G.L., Dissard, D., Gage,
806 J.D., Hughes, D.J., Jeffreys, R., Lamont, P.A., Larkin, K.E., Murty, S.J.,
807 Schumacher, S., Whitcraft, C., Woulds, C., 2009. Faunal responses to oxygen
808 gradients on the Pakistan margin: A comparison of foraminiferans, macrofauna
809 and megafauna. Deep-Sea Research II 56, 488-502.
810 Gromet, L.P., Dymek, R.F., Haskin, L.A., Korotev, R.L., 1984. The "North American
811 shale composite": Its compilation, major and trace element characteristics.
812 Geochimica et Cosmochimica Acta 48, 2469-2482.
813 Hofmann, A., Peltzer, E., Walz, P., Brewer, P., 2011. Hypoxia by degrees: Establishing
814 definitions for a changing ocean. Deep Sea Research Part I: Oceanographic
815 Research Papers 58, 1212-1226.
816 Holland, H.D., Beukes, N.J., 1990. A paleoweathering profile from Griqualand West,
817 South Africa: evidence for a dramatic rise in atmospheric oxygen between 2.2 and
818 1.9 bybp. American Journal of Science 290A, 1-34.
819 Ingole, B.S., Sautya, S., Sivadas, S., Singh, R., Nanajkar, M., 2010. Macrofaunal
820 community structure in the western Indian continental margin including the
821 oxygen minimum zone. Marine Ecology 31, 148-166.

822 Jeffreys, R.M., Levin, L.A., Lamont, P.A., Woulds, C., Whitcraft, C.R., Mendoza, G.F.,
823 Wolff, G.A., Cowie, G.L., 2012. Living on the edge: single-species dominance at
824 the Pakistan oxygen minimum zone boundary. Marine Ecology Progress Series
825 470, 79-99.
826 Johnston, D.T., Poulton, S.W., Dehler, C.M., Porter, S., Husson, J., Canfield, D.E., Knoll,
827 A.H., 2010. An emerging picture of Neoproterozoic ocean chemistry: Insights
828 from the Chuar Group, Grand Canyon, USA. Earth and Planetary Science Letters
829 290, 64-73.
830 Johnston, D.T., Fischer, W.W., 2012. Stable isotope geobiology, in: Knoll, A.H.,
831 Canfield, D.E., Konhauser, K.O. (Eds.), Fundamentals of Geobiology.
832 Blackwells, Chichester, pp. 250-266.
833 Kah, L.C., Bartley, J.K., 2011. Protracted oxygenation of the Proterozoic biosphere.
834 International Geology Review 53, 1424-1442.
835 Karlstrom, K.E., Bowring, S.A., Dehler, C.M., Knoll, A.H., Porter, S.M., Des Marais,
836 D.J., Weil, A.B., Sharp, Z.D., Geissman, J.W., Elrick, M.B., 2000. Chuar Group
837 of the Grand Canyon: Record of breakup of Rodinia, associated change in the
838 global carbon cycle, and ecosystem expansion by 740 Ma. Geology 28, 619-622.
839 King, N., Westbrook, M.J., Young, S.L., Kuo, A., Abedin, M., Chapman, J., Fairclough,
840 S., Hellsten, U., Isogai, Y., Letunic, I., Marr, M., Pincus, D., Putnam, N., Rokas,
841 A., Wright, K.J., Zuzow, R., Dirks, W., Good, M., Goodstein, D., Lemons, D., Li,
842 W., Lyons, J.B., Morris, A., Nichols, S., Richter, D.J., Salamov, A., Sequencing,
843 J., Bork, P., Lim, W.A., Manning, G., Miller, W.T., McGinnis, W., Shapiro, H.,
844 Tijan, R., Grigoriev, I.V., Rokhsar, D., 2008. The genome of the choanoflagellate
845 Monosiga brevicollis and the origin of metazoans. Nature 451, 783-788.
846 Knoll, A.H., 2011. The multiple origins of complex multicellularity. Annual Review of
847 Earth and Planetary Sciences 39, 217–239.
848 Knoll, A.H., Bambach, R.K., Payne, J.L., Pruss, S., Fischer, W., 2007. Paleophysiology
849 and end-Permian mass extinction. Earth and Planetary Science Letters 256, 295-
850 313.
851 Knoll, A.H., Carroll, S.B., 1999. Early animal evolution: Emerging views from
852 comparative biology and geology. Science 284, 2129-2137.
853 Knoll, A.H., Javaux, E.J., Hewitt, D., Cohen, P., 2006. Eukaryotic organisms in
854 Proterozoic oceans. Philosophical Transactions of the Royal Society London
855 Series B 361, 1023-1038.
856 Kodner, R.B., Summons, R.E., Pearson, A., King, N., and Knoll, A.H., 2008. Sterols in a
857 unicellular relative of the metazoans. Proceedings of the National Academy of
858 Sciences, USA 105, 9897-9902.
859 Kump, L.R., 2008. The rise of atmospheric oxygen. Nature 451, 277-278.
860 Kump, L.R., Pavlov, A., Arthur, M.A., 2005. Massive release of hydrogen sulfide to the
861 surface ocean and atmosphere during intervals of oceanic anoxia. Geology 33,
862 397-400.
863 Lamont, P.A., Gage, J.D., 2000. Morphological responses of macrobenthic polychaetes to
864 low oxygen on the Oman continental slope, NW Arabian Sea. Deep-Sea Research
865 II 47, 9-24.

866 Lartillot, N., Lepage, T., Blanquart, S., 2009. PhyloBayes 3: a Bayesian software package
867 for phylogenetic reconstruction and molecular dating. Bioinformatics 25, 2286-
868 2288.
869 Levin, L., Ekau, W., Gooday, A., Jorissen, F., Middelburg, J., Naqvi, W., Neira, C.,
870 Rabalais, N., Zhang, J., 2009. Effects of natural and human-induced hypoxia on
871 coastal benthos. Biogeosciences Discussions 6, 3563-3654.
872 Levin, L., Gutierrez, D., Rathburn, A., Neira, C., Sellanes, J., Munoz, P., Gallardo,
873 V., Salamanca, M., 2002. Benthic processes on the Peru margin: a transect across
874 the oxygen minimum zone during the 1997-98 El Niño. Progress in
875 Oceanography 53, 1-27.
876 Levin, L.A., 2003. Oxygen Minimum Zone benthos: adaptation and community response
877 to hypoxia. Oceanography and Marine Biology: an Annual Review 41, 1-45.
878 Levin, L.A., Huggett, C.L., Wishner, K.F., 1991. Control of deep-sea benthic community
879 structure by oxygen and organic-matter gradients in the eastern Pacific Ocean.
880 Journal of Marine Research 49, 763-800.
881 Love, G.D., Grosjean, E., Stalvies, C., Fike, D.A., Grotzinger, J.P., Bradley, A.S., Kelly,
882 A.E., Bhatia, M., Meredith, W., Snape, C.E., Bowring, S.A., Condon, D.J.,
883 Summons, R.E., 2009. Fossil steroids record the appearance of Demospongiae
884 during the Cryogenian period. Nature 457, 718-721.
885 Lyons, T.W., Severmann, S., 2006. A critical look at iron paleoredox proxies: New
886 insights from modern euxinic marine basins. Geochimica et Cosmochimica Acta
887 70, 5698-5722.
888 Macdonald, F.A., Halverson, G.P., Strauss, J.V., Smith, E.F., Cox, G., Sperling, E.A.,
889 Roots, C.F., 2012. Early Neoproterozoic basin formation in the Yukon:
890 implications for the make-up and break-up of Rodinia. Geoscience Canada 39,
891 77-99.
892 Macdonald, F.A., Schmitz, M.D., Crowley, J.L., Roots, C.F., Jones, D.S., Maloof, A.C.,
893 Strauss, J.V., Cohen, P.A., Johnston, D.T., Schrag, D.P., 2010. Calibrating the
894 Cryogenian. Science 327, 1241-1243.
895 Nagy, R.M., Porter, S.M., Dehler, C.M., Shen, Y., 2009. Biotic turnover driven by
896 eutrophication before the Sturtian low-latitude glaciation. Nature Geoscience 2,
897 415-418.
898 Narbonne, G.M., 2011. When life got big. Nature 470, 339-340.
899 Neira, C., Gad, G., Arroyo, N.L., Decraemer, W., 2001. Glochinema bathyperuvensis sp.
900 n. (Nematoda, Epsilonematidae): a new species from Peruvian bathyal sediments,
901 SE Pacific Ocean. Contributions to Zoology 70, 147-159.
902 Nesbitt, H., Young, G., 1982. Early Proterozoic climates and plate motions inferred from
903 major element chemistry of lutites. Nature 299, 715-717.
904 Och, L.M., Shields-Zhou, G.A., 2012. The Neoproterozoic oxygenation event:
905 environmental perturbations and biogeochemical cycling. Earth Science Reviews
906 110, 26-57.
907 Palma, M., Quiroga, E., Gallardo, V.A., Arntz, W., Gerdes, D., Schneider, W., Hebbeln,
908 D., 2005. Macrobenthic animal assemblages of the continental margin off Chile
909 (22° to 42° S). Journal of the Marine Biological Association of the UK 85, 233-
910 245.

911 Parfrey, L.W., Lahr, D.J.G., Knoll, A.H., Katz, L.A., 2011. Estimating the timing of early
912 eukaryotic diversification with multigene molecular clocks. Proceedings of the
913 National Academy of Sciences, U.S.A. 108, 13624-13629.
914 Paulmier, A., Ruiz-Pino, D., Garçon, V., Farias, L., 2006. Maintaining of the eastern
915 south Pacific oxygen minimum zone (OMZ) off Chile. Geophysical Research
916 Letters 33, L20601.
917 Pavlov, A., Kasting, J., 2002. Mass-independent fractionation of sulfur isotopes in
918 Archean sediments: strong evidence for an anoxic Archean atmosphere.
919 Astrobiology 2, 27-41.
920 Payne, J.L., McClain, C.R., Boyer, A.G., Brown, J.H., Finnegan, S., Kowalewski, M.,
921 Krause, J.R.A., Lyons, S.K., McShea, D.W., Novack-Gottshall, P.M., Smith,
922 F.A., Spaeth, P., Stempien, J.A., Wang, S.C., 2010. The evolutionary
923 consequences of oxygenic photosynthesis: a body size perspective.
924 Photosynthesis Research 107, 37-57.
925 Peters, S.E., Loss, D.P., 2012. Storm and fair-weather wave base: A relevant distinction?
926 Geology 40, 511-514.
927 Philippe, H., Brinkmann, H., Lavrov, D.V., Littlewood, D.T.J., Manuel, M., Worheide,
928 G., Baurain, D., 2011. Resolving difficult phylogenetic questions: why more
929 sequences are not enough. PLoS Biology 9, e1000602.
930 Philippe, H., Derelle, R., Lopez, P., Pick, K., Borchiellini, C., Boury-Esnault, N.,
931 Vacelet, J., Deniel, E., Houliston, E., Queinnec, E., Da Silva, C., Wincker, P., Le
932 Guyader, H., Leys, S., Jackson, D.J., Scheiber, F., Erpenbeck, D., Morgenstern,
933 B., Worheide, G., Manuel, M., 2009. Phylogenomics restores traditional views on
934 deep animal relationships. Current Biology 19, 706-712.
935 Planavsky, N.J., Rouxel, O.J., Bekker, A., Lalonde, S.V., Konhauser, K.O., Reinhard,
936 C.T., Lyons, T.W., 2010. The evolution of the marine phosphate reservoir. Nature
937 467, 1088-1090.
938 Porter, S.M., Knoll, A.H., 2000. Testate amoeba in the Neoproterozoic Era: evidence
939 from vase-shaped microfossils in the Chuar Group, Grand Canyon. Paleobiology
940 26, 360-385.
941 Porter, S.M., Meisterfeld, R., Knoll, A.H., 2003. Vase-shaped microfossils from the
942 Neoproterozoic Chuar Group, Grand Canyon: a classification guided by modern
943 testate amoebae. Journal of Paleontology 77: 205-225.
944 Poulton, S., Raiswell, R., 2002. The low-temperature geochemical cycle of iron: from
945 continental fluxes to marine sediment deposition. American Journal of Science
946 302, 774-805.
947 Poulton, S.W., Canfield, D.E., 2005. Development of a sequential extraction procedure
948 for iron: implications for iron partitioning in continentally derived particulates.
949 Chemical Geology 214, 209-221.
950 Poulton, S.W., Canfield, D.E., 2011. Ferruginous conditions: A dominant feature of the
951 ocean through Earth's history. Elements 7, 107-112.
952 Prockop, D., Kaplan, A., Udenfriend, S., 1963. Oxygen-18 studies on the conversion of
953 proline to collagen hydroxyproline. Archives of Biochemistry and Biophysics
954 101, 499-503.
955 Raff, R.A., Raff, E.C., 1970. Respiratory mechanisms and the metazoan fossil record.
956 Nature 228, 1003-1005.

957 Rainbird, R.H., Jefferson, C.W., Young, G.M., 1996. The early Neoproterozoic
958 sedimentary Succession B of northwestern Laurentia: Correlations and
959 paleogeographic significance. Geological Society of America Bulletin 108, 454-
960 470.
961 Raiswell, R., Canfield, D.E., 1998. Sources of iron for pyrite formation in marine
962 sediments. American Journal of Science 298, 219-245.
963 Rhoads, D.C., Morse, J.W., 1971. Evolutionary and ecologic significance of oxygen-
964 deficient marine basins. Lethaia 4, 413-428.
965 Runnegar, B., 1982a. The Cambrian explosion: animals or fossils? Journal of the
966 Geological Association of Australia 29, 395-411.
967 Runnegar, B., 1982b. Oxygen requirements, biology and phylogenetic significance of the
968 late Precambrian worm *Dickinsonia*, and the evolution of the burrowing habit.
969 Alcheringa 6, 223-239.
970 Runnegar, B., 1991. Precambrian oxygen levels estimated from the biochemistry and
971 physiology of early eukaryotes. Palaeogeography, Palaeoclimatology,
972 Palaeoecology 97, 97-111.
973 Ruppert, E.E., Fox, R.S., Barnes, R.D., 2004. Invertebrate Zoology. Thomson, Belmont,
974 CA. p. 1-963.
975 Sahoo, S.K., Planavsky, N.J., Kendall, B., Wang, X., Shi, X., Scott, C., Anbar, A.D.,
976 Lyons, T.W., Jiang, G., 2012. Ocean oxygenation in the wake of the Marinoan
977 glaciation. Nature 489, 546- 549.
978 Scott, C., Lyons, T.W., Bekker, A., Shen, Y., Poulton, S.W., Chu, X., Anbar, A.D., 2008.
979 Tracing the stepwise oxygenation of the Proterozoic ocean. Nature 452, 456-459.
980 Shen, Y., Knoll, A.H., Walter, M.R., 2003. Evidence for low sulphate and anoxia in a
981 mid-Proterozoic marine basin. Nature 423, 632-635.
982 Sperling, E.A., Peterson, K.J., Pisani, D., 2009. Phylogenetic-signal dissection of nuclear
983 housekeeping genes supports the paraphyly of sponges and the monophyly of
984 Eumetazoa. Molecular Biology and Evolution 26, 2261-2274.
985 Sperling, E.A., Robinson, J.M., Pisani, D., Peterson, K.J., 2010. Where's the glass?
986 Biomarkers, molecular clocks, and microRNAs suggest a 200-Myr missing
987 Precambrian fossil record of siliceous sponges. Geobiology 8, 24-36.
988 Sperling, E.A., Frieder, C.A., Raman, A., Girguis, P.R., Levin, L.A., Knoll, A.H., in
989 review. Oxygen, ecology, and the Cambrian radiation of animals. Nature
990 Geoscience.
991 Terwilliger, N.B., 1998. Functional adaptations of oxygen-transport proteins. Journal of
992 experimental biology 201, 1085-1098.
993 Thorkelson, D.J., Abbott, J.G., Mortensen, J.K., Creaser, R.A., Velleneuve, M.E.,
994 McNicoll, V.J., Layer, P.W., 2005. Early and Middle Proterozoic evolution of
995 Yukon, Canada. Canadian Journal of Earth Sciences 42, 1045-1071.
996 Tribovillard, N., Algeo, T.J., Lyons, T., Riboulleau, A., 2006. Trace metals as paleoredox
997 and paleoproductivity proxies: An update. Chemical Geology 232, 12-32.
998 Towe, K.M., 1970. Oxygen-collagen priority and the early metazoan fossil record.
999 Proceedings of the National Academy of Sciences, U.S.A. 65, 781-788.
1000 Tyson, R.V., Pearson, T.H., 1991. Modern and ancient continental shelf anoxia: an
1001 overview, in: Tyson, R.V., Pearson, T.H. (Eds.), Modern and Ancient Continental
1002 Shelf Anoxia. Geological Society Special Publications, London, pp. 1-24.

1003 Vaquer-Sunyer, R., Duarte, C.M., 2008. Thresholds of hypoxia for marine biodiversity.
1004 Proceedings of the National Academy of Sciences 105, 15452-15457.
1005 Wang, C., Leger, R.J.S., 2006. A collagenous protective coat enables Metarhizium
1006 anisopliae to evade insect immune responses. Proceedings of the National
1007 Academy of Sciences 103, 6647-6652.
1008 Zettler, M.L., Bochert, R., Pollehne, F., 2009. Macrozoobenthos diversity in an oxygen
1009 minimum zone off northern Namibia. Marine Biology 156, 1949-1961.

HARVARD UNIVERSITY
DEPARTMENT OF EARTH AND PLANETARY SCIENCES
20 OXFORD ST.
CAMBRIDGE, MA 02138
TEL. (617) 495-2351 FAX. (617) 495-8839

Highlights for Sperling *et al*.

1) We present the first early Neoproterozoic basin redox transect

2) Redox proxy data are consistent with quantitative constraints on Proterozoic O_2

3) Inferred Proterozoic oxygen levels would not prohibit the presence of animals

Figure 1

Click here to download Figure: Figure 1 Locality map.pdf

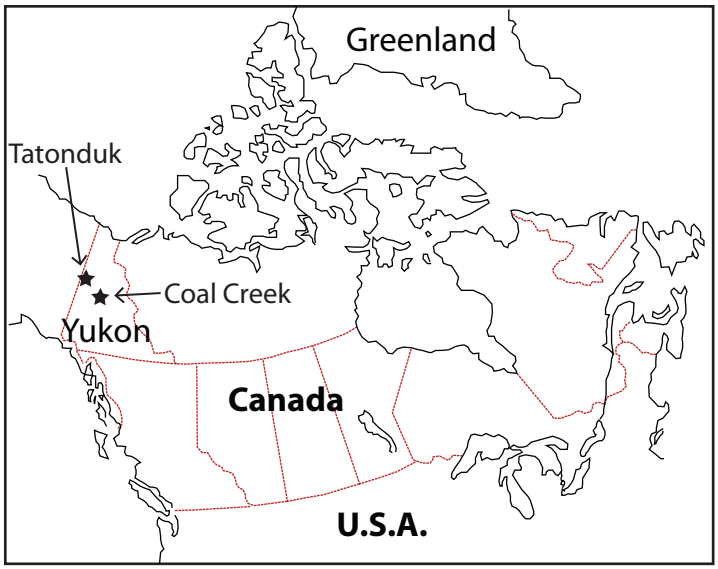

Figure 2
Click here to download Figure: Figure 2 Coal_Creek_Erik_Sandford

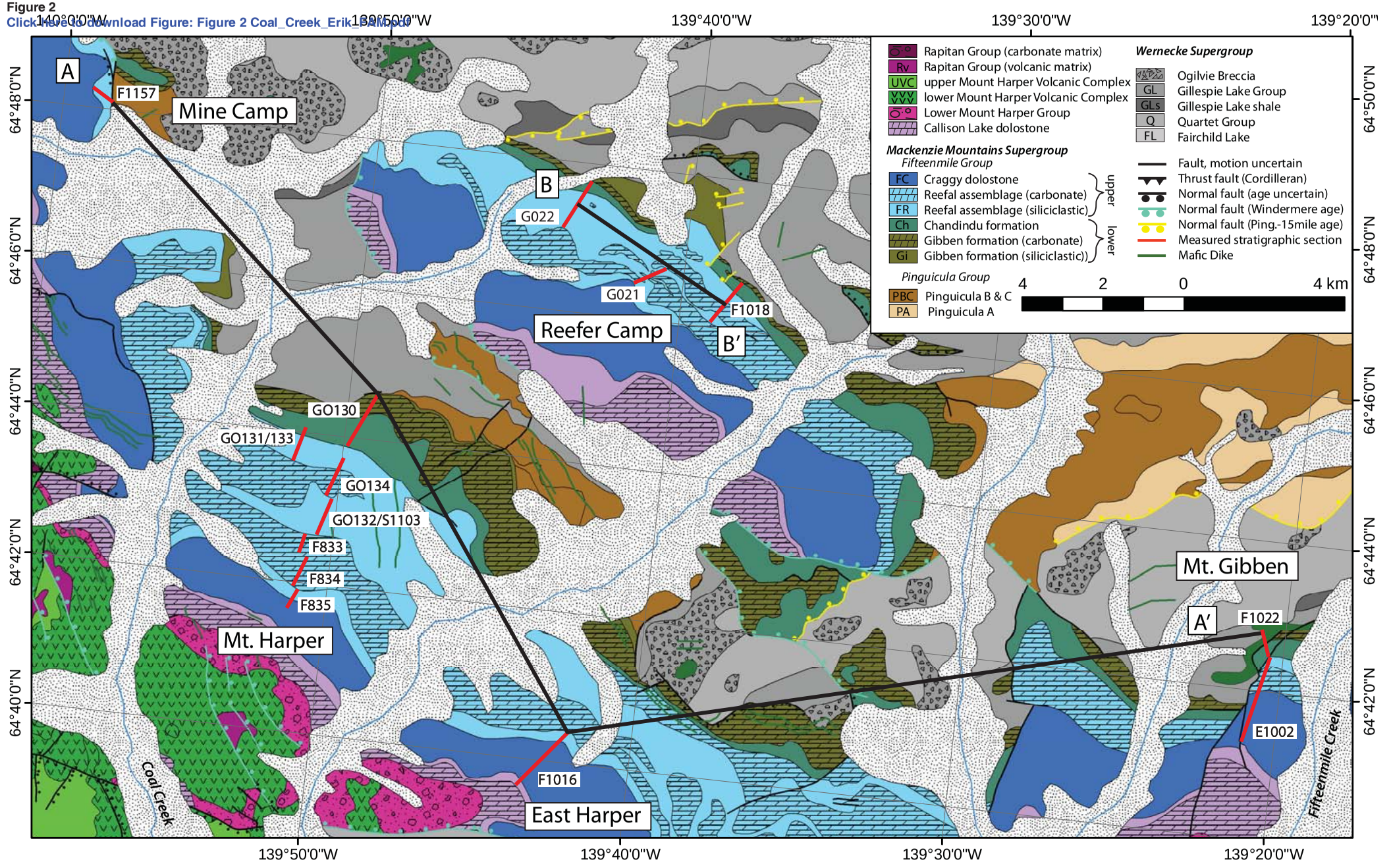

Figure 3

Click here to download Figure: Figure 3 Fifteenmile iron speciation_long transect_revised.pdf

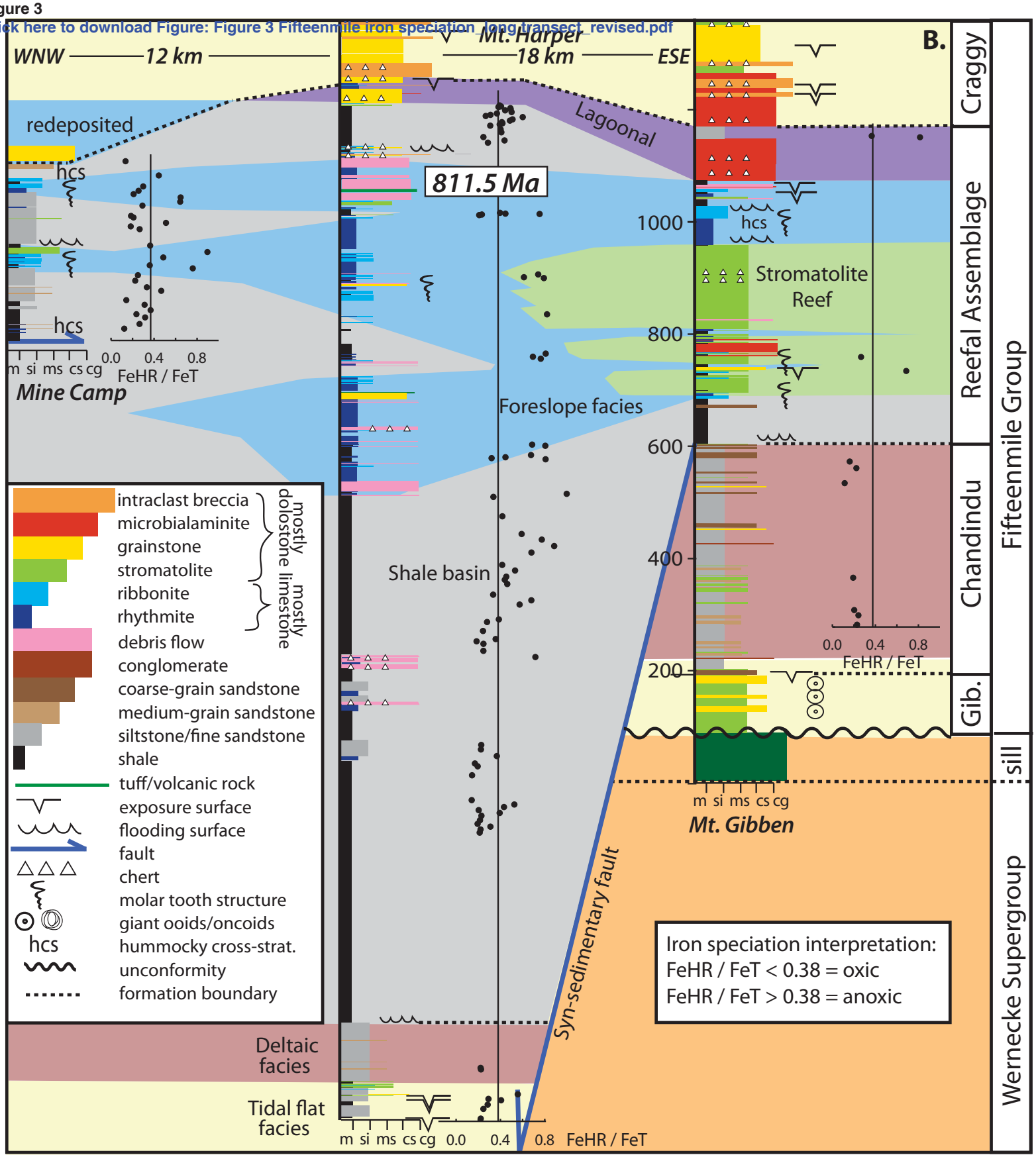

Figure 4

Click here to download Figure: Figure 4 Fifteenmile iron speciation_revised.pdf

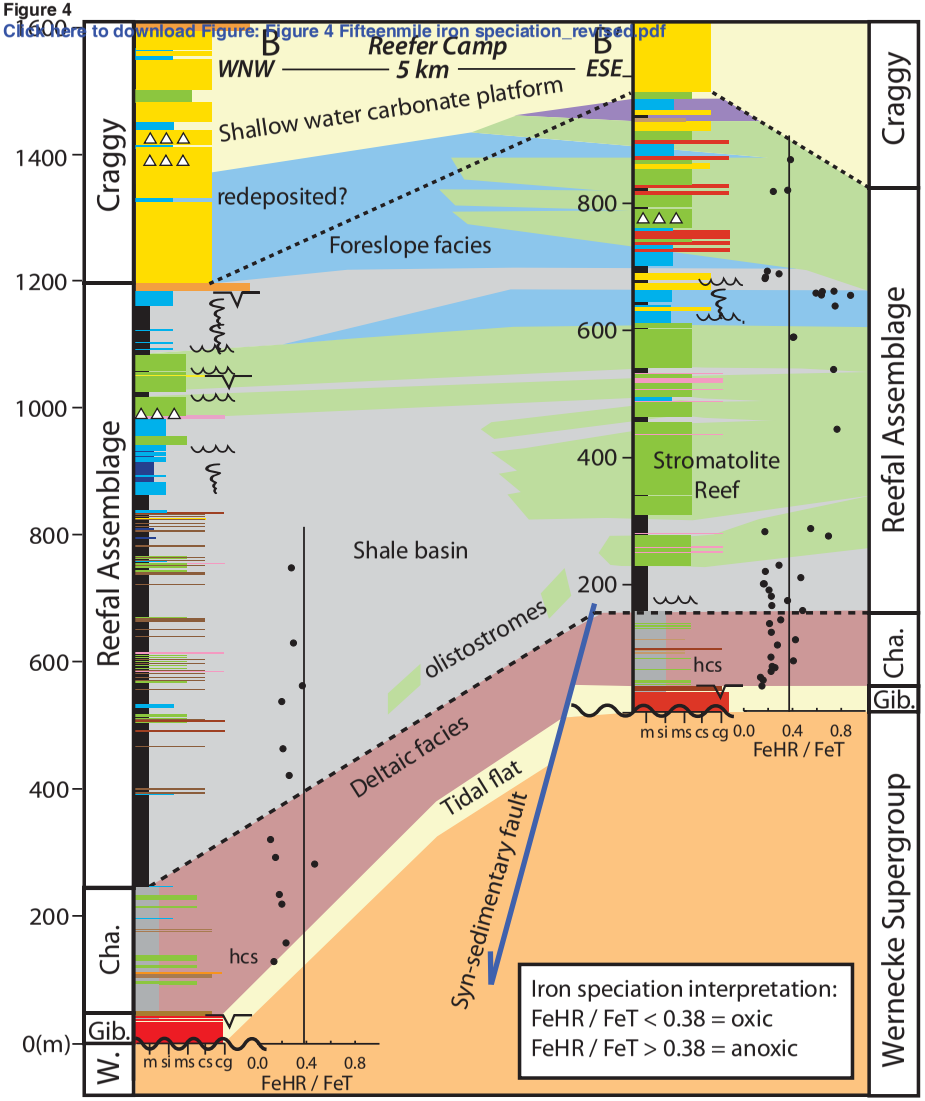

Figure 5

Click here to download Figure: Figure 5 Reefer Geochemistry Full_revised.pdf

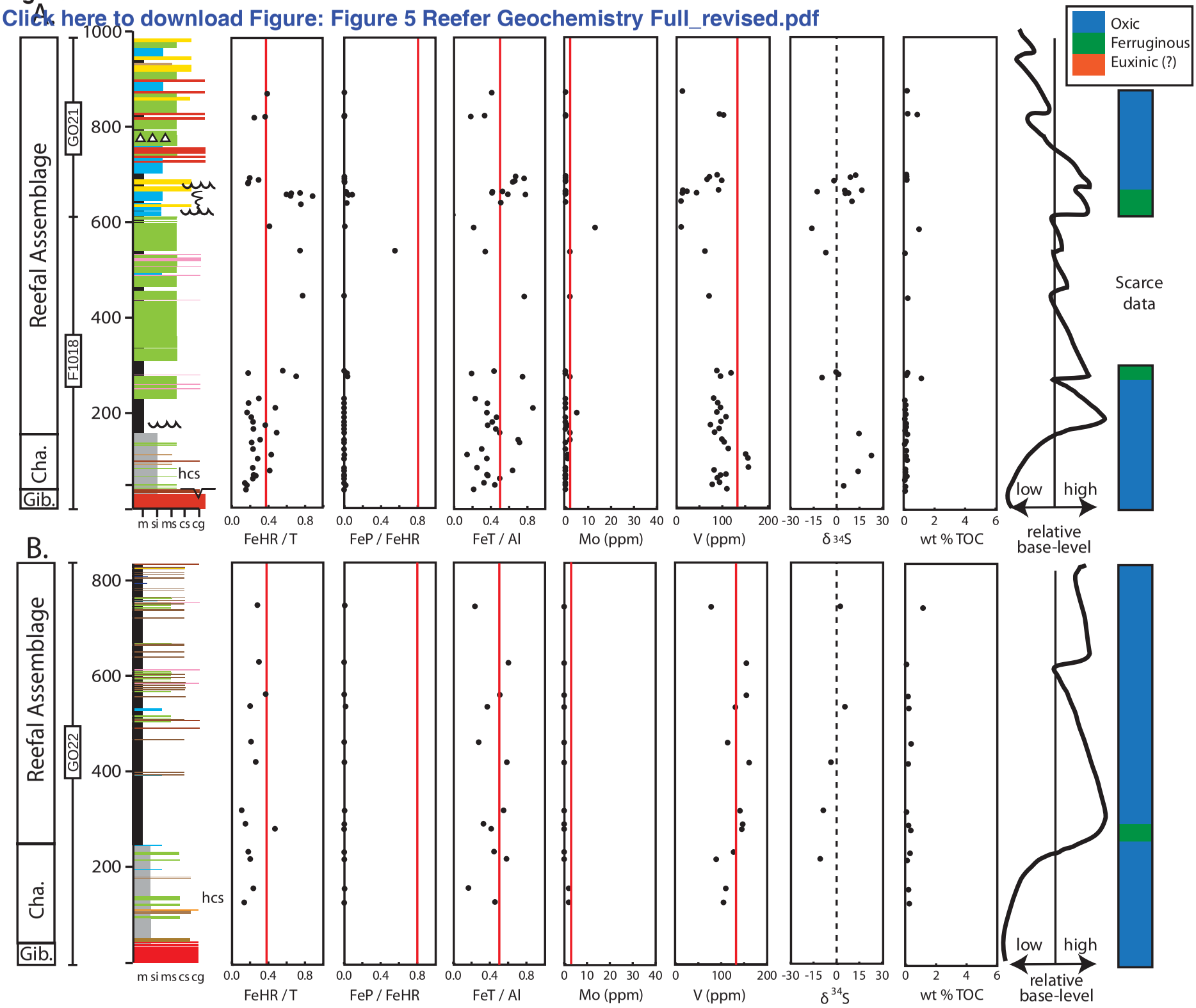

Figure 6

Click here to download Figure: Figure 6 Harper composite full geochemistry_revised.pdf

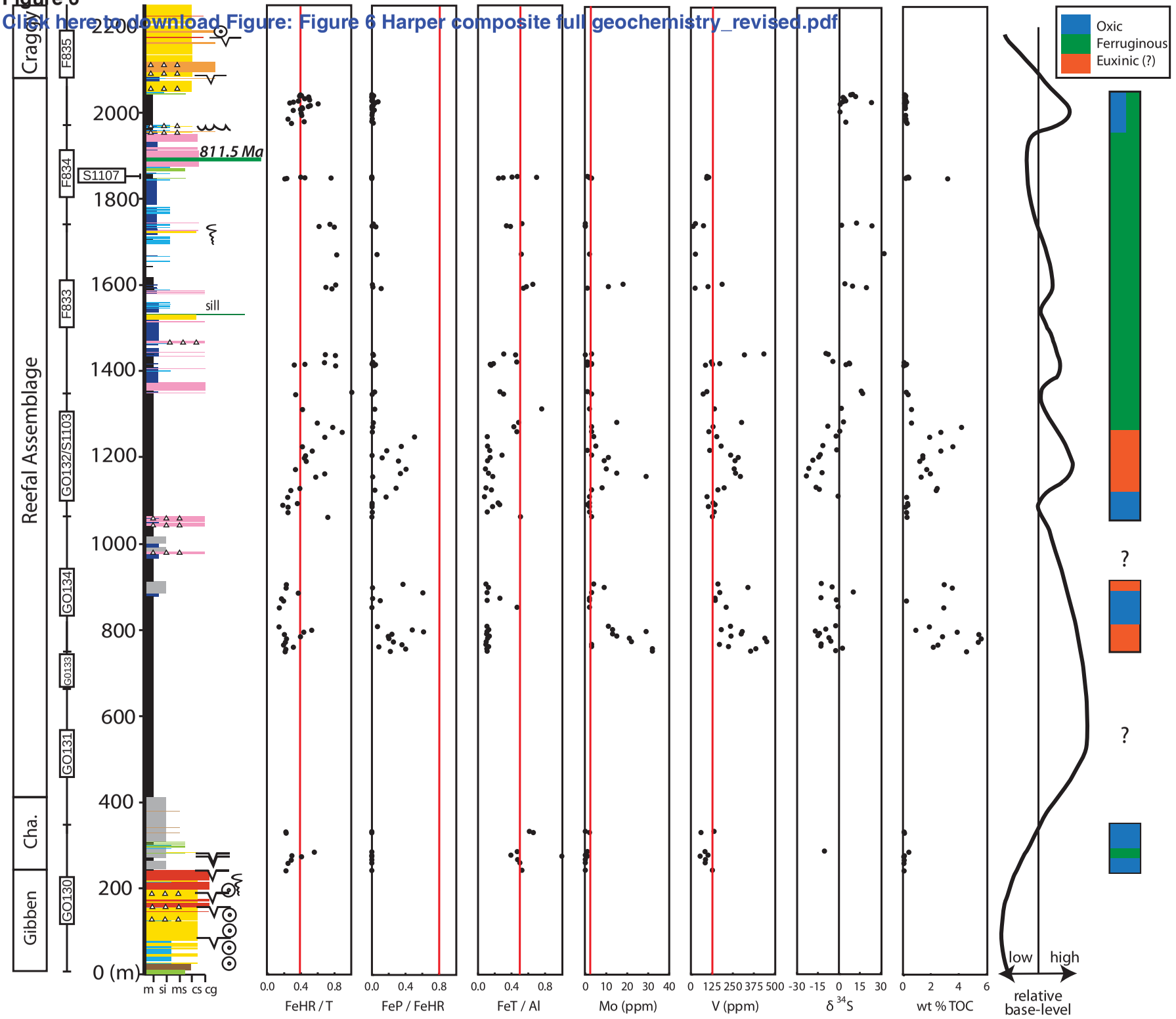

Figure 7

Click here to download Figure: Figure 7 Tindir Geochemistry Full_revised.pdf

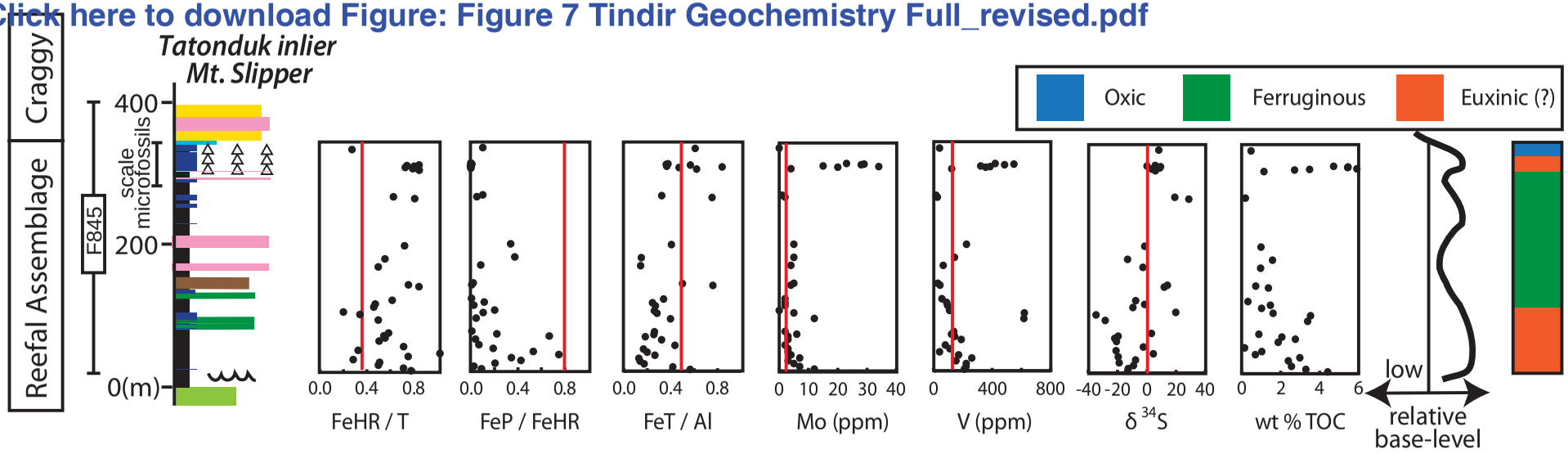

Figure 8
Click here to download Figure: Figure 8 Ferruginous Euxinic boxplot.pdf

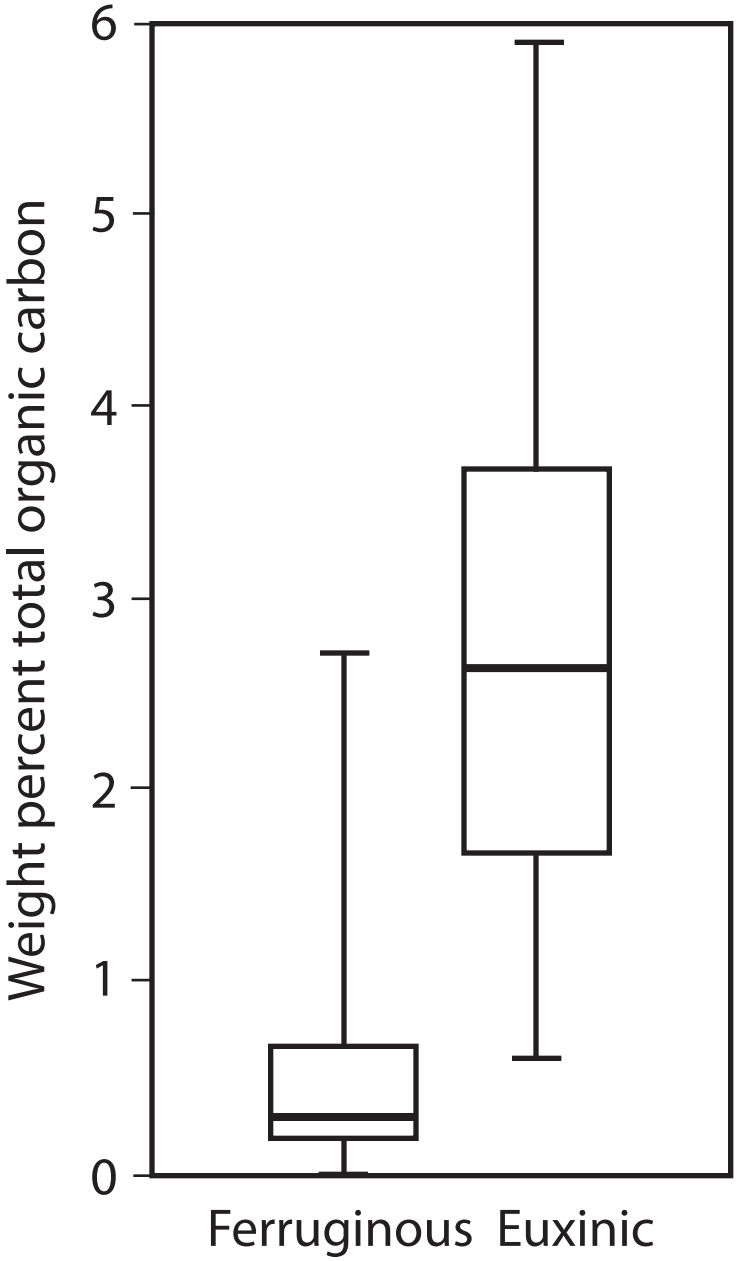

Figure 9

Click here to download Figure: Figure 9 Bilaterian oxygen requirements figure.pdf